COMMUNICATION

Ultrathin films of porous metal-organic polyhedra for gas separation

Miguel A. Andrés[a,b], Arnau Carné-Sánchez[c], Javier Sánchez-Laínez[b,d], Olivier Roubeau[b], Joaquín Coronas[b,d], Daniel Maspoch*[c,e], Ignacio Gascón*[a,b]

Abstract: Ultrathin films of a robust Rh(II)-based porous metal-organic polyhedra (MOP) have been obtained. Homogeneous and compact monolayer films (*ca.* 2.5 nm thick) were first formed at the air-water interface, deposited onto different substrates and characterized using spectroscopic methods, scanning transmission electron microscopy and atomic force microscopy. As a proof of concept, the gas separation performance of MOP supported membranes has been also evaluated. Selective MOP ultrathin films (thickness *ca.* 60 nm) exhibit remarkable CO_2 permeance and CO_2/N_2 selectivity, demonstrating the great combined potential of MOP and Langmuir-based techniques in separation technologies.

The current technology for capturing CO_2 at the emission points relies on its absorption in alkanolamine aqueous solutions. This solution-based method is highly selective but requires high regeneration temperatures, which reduces its recyclability and increases its cost making difficult its implementation at large scale.[1] Alternatively, CO_2 separation by membranes has emerged as an environmentally friendly and more cost effective method,[2] and can be applied to other processes of interest such as the upgrading of biogas to biomethane.[3] However, current membranes lack the capacity to treat huge amounts of flue gas with the required selectivity for CO_2.[4] Accordingly, membranes able to achieve high gas flux (permeance) while maintaining a high selectivity for CO_2 are intensively sought. One way of increasing gas flux is decreasing the thickness of the membrane because both parameters are inversely proportional. Therefore, ultrathin porous films with thicknesses below 100 nm have the potential to enhance membrane performance by increasing the flux of gas through the membrane without losing CO_2 selectivity.[5, 6] Langmuir-Blodgett (LB) is a technique especially suitable for this purpose as it enables the self-assembly of a wide range of molecules/nanocrystals into dense monolayers.[7] The subsequent transfer of such films to permeable supports opens the possibility to fabricate multilayer membranes with precise control on the thickness of the selective layer.[8] However, this potential remains under-exploited because the majority of porous materials lack the solution processability required for the LB method. Accordingly, the use of the LB technique to fabricate ultrathin membranes for CO_2 capture has been restricted to soluble organic molecules[8] and polymers of intrinsic porosity (PIMs).[9]

Herein, we expand the scope of the LB method to discrete metal-organic polyhedral molecules (MOPs) fabricating MOP-based ultrathin films. MOPs are nanosized molecules of 2-5 nm synthesised from the self-assembly of metal ions and organic linkers, which can be soluble in different polar and non-polar liquids and permanently porous in solid state.[10-14] In this communication, we show how robust Rh(II)-based MOPs can be assembled at the air-water interface through the LB technique forming homogenous 2-3 nm thick monolayer films. For this study, we selected a cuboctahedral Rh-MOP functionalized with pendant aliphatic chains with formula: $[Rh_2(C_{12}\text{-bdc})_2]_{12}$ (hereafter C_{12}RhMOP; C_{12}-bdc = 5-dodecoxybenzene-1,3-dicarboxylate; Figure 1a) due to its hydrolytic stability and good solubility in organic solvents such as dichloromethane (DCM).[15,16] High hydrolytic stability of MOPs is a prerequisite for the LB method because the assembled monolayers are formed on top of the water phase. Thus, MOPs based on labile coordination bonds such as Cu(II)-carboxylate were not considered for this study. Furthermore, the pendant aliphatic chains of C_{12}RhMOP are expected to facilitate the formation of a compact monolayer at the air-water interface and to favour the cohesion among deposited multilayers. Moreover, previous studies[16] have shown that C_{12}RhMOP displays a negligible N_2 adsorption at 77 K (0.17 and 0.82 N_2 moles per MOP mol at $P/P_0 \approx 0.1$ and $P/P_0 \approx 0.95$, respectively) and a significant CO_2 adsorption at 195 K (9 and 22 mol of CO_2 per MOP mol at $P/P_0 \approx 0.1$ and $P/P_0 \approx 0.95$, respectively), making it an interesting candidate for CO_2/N_2 separation. Multiple C_{12}RhMOP monolayer films were thus deposited on the permeable polymer poly[1-(trimethylsilyl)-1-propyne] (PTMSP) to fabricate a multilayer membrane with the desired MOP film thickness. The CO_2/N_2 selectivity of the PTMSP membrane at 1 bar and 35°C was significantly increased from 4.1 to 10.1 after 30 deposition cycles of C_{12}RhMOP monolayers while keeping high the CO_2 permeance (195 GPU), thereby demonstrating the potential of molecularly thin MOP films for the CO_2/N_2 separation.

[a] M. A. Andrés, Dr. I Gascón
Departamento de Química Física and Instituto de Nanociencia de Aragón (INA), Universidad de Zaragoza, 50009 Zaragoza (Spain).
E-mail: igascon@unizar.es
[b] M. A. Andrés, Dr. J. Sánchez-Laínez, Dr. Olivier Roubeau, Prof. Dr. J. Coronas, Dr. I Gascón
Instituto de Ciencia de Materiales de Aragón (ICMA), CSIC and Universidad de Zaragoza, 50009 Zaragoza, Spain.
[c] Dr. A. Carné-Sánchez, Prof. Dr. D. Maspoch
Catalan Institute of Nanoscience and Nanotechnology (ICN2), CSIC and The Barcelona Institute of Science and Technology, Campus UAB, Bellaterra, 08193 Barcelona, Spain.
E-mail: daniel.maspoch@icn2.cat
[d] Dr. J. Sánchez-Laínez, Prof. Dr. J. Coronas
Chemical and Environmental Engineering Department and Instituto de Nanociencia de Aragón (INA) Universidad de Zaragoza, 50018 Zaragoza, Spain
[e] Prof. Dr. D. Maspoch
ICREA, Pg. Lluís Companys 23, 08010 Barcelona, Spain

Supporting information for this article is given via a link at the end of the document.

COMMUNICATION

We initially prepared a diluted $C_{12}RhMOP$ solution in DCM ($2.8\cdot10^{-6}$ M) to study Langmuir film formation. Then, 1000 - 1200 µL of the $C_{12}RhMOP$ solution (i.e. the total mass of $C_{12}RhMOP$ employed was 0.04 mg) were spread on the water subphase. After solvent evaporation (*ca.* 10 min), the floating molecules were compressed to induce their assembly into a monolayer film (Figure 1b). The surface pressure - area isotherm (π-A) reveals that the self-assembly process starts when $C_{12}RhMOP$ is compressed to an area of 8 nm^2/molecule (Figure 1c). Further compression causes a steep increase of the surface pressure indicating the formation of the film. The maximum slope at *ca.* 5 nm^2/molecule is in good agreement with the estimated lateral size of a single molecule with extended alkyl substituents at *ca.* 5.3 nm (see Figure S1 in the Supporting Information), which would indicate that the film formation involves a partial interdigitation of the alkyl arms. Brewster angle microscopy images obtained during $C_{12}RhMOP$ compression reveal that the water surface is completely covered by a $C_{12}RhMOP$ monolayer film at a surface pressure of 25 $mN\cdot m^{-1}$ (see Figure S2 in the Supporting Information). Increasing the surface pressure above 37.5 $mN\cdot m^{-1}$ causes the collapse of the $C_{12}RhMOP$ film, which agrees with the change in the slope of the surface pressure in the π-A isotherm and the value determined from the surface potential measurements (see Figure S3 in the Supporting Information).
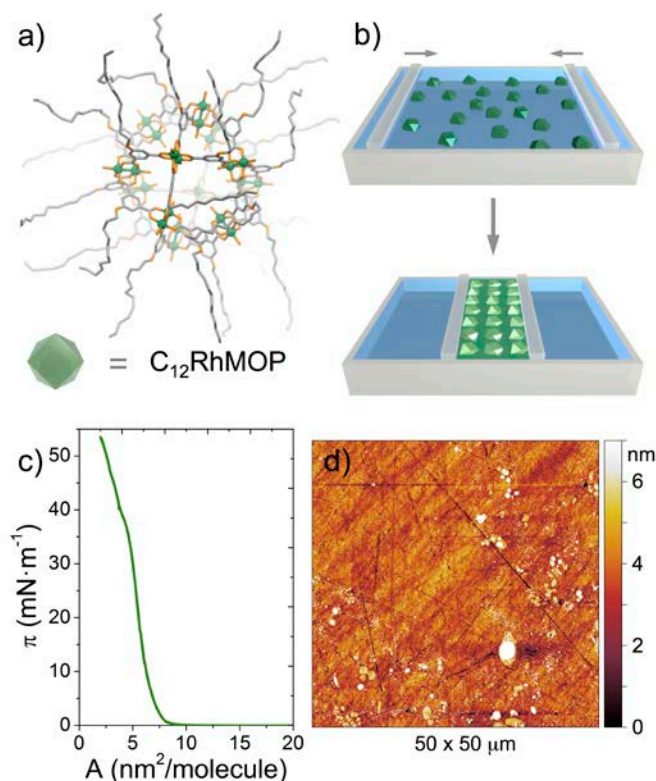
Figure 1 (a) View of the $C_{12}RhMOP$ molecule based on the crystal structure of the related $C_{12}CuMOP$ and its schematic representation as a cuboctahedron.[17] Colour code: Rh (green), C (grey), O (orange). (b) Scheme of the formation of a continuous Langmuir film upon compression of $C_{12}RhMOP$ molecules expanded at the air-water interface. (c) π-A isotherm obtained from the compression of $C_{12}RhMOP$. (d) AFM image of a single monolayer of $C_{12}RhMOP$ deposited on quartz substrate. Note here that the observed scratches correspond to defects on the surface of the quartz plates used since phase images confirmed that the samples were homogeneous.

Next, monolayer films compressed at surface pressures between 15 and 35 $mN\cdot m^{-1}$ were transferred onto mica and quartz substrates. Two different deposition methods were tested: vertical transfer (Langmuir-Blodgett films) and horizontal transfer (Langmuir-Schaefer, LS, films). Irrespectively of the deposition method employed, the UV-Vis spectra of the $C_{12}RhMOP$ deposited on quartz reveal the presence of two bands at 265 and 315 nm, which are in perfect agreement with the UV-Vis spectra of $C_{12}RhMOP$ in solution. This confirms the stability of $C_{12}RhMOP$ throughout the whole assembly process (see Figure S4 in the Supporting Information).

However, the absorbance values obtained for the monolayer films transferred horizontally are systematically higher than for those transferred vertically, at all pressures tested, thereby suggesting a better quality and homogeneity for the LS films (see Figure S5 in the Supporting Information). UV-Vis measurements also indicate that the film absorbance values are lower when surface pressures above 25 $mN\cdot m^{-1}$ are employed. These low absorbance values reflect a poorer film coverage, probably because the film becomes too rigid above this surface pressure, making the transfer less effective. These observations are in line with atomic force microscopy (AFM) measurements, as complete substrate coverage is achieved when monolayer films are transferred at a surface pressure of 25 $mN\cdot m^{-1}$ (Figure 1d and Figures S6 and S7 in the Supporting Information). On the contrary, a lower film coverage is observed when transfers were performed at 35 $mN\cdot m^{-1}$, due to the presence of domains with different thicknesses. Altogether, these results confirm that horizontal transfer at a surface pressure of 25 $mN\cdot m^{-1}$ allows the formation of homogeneous LS $C_{12}RhMOP$ monolayer films on surfaces with an average height of *ca.* 2.5 nm (see Figure 1d and Figure S7 in the Supporting Information). Interestingly, no significant differences in terms of homogeneity are observed when using different types of flat substrates, i.e. the hydrophilic inorganic mica or quartz or the hydrophobic PTSMP organic polymer (see below).

With the pressure and the deposition method of $C_{12}RhMOP$ monolayers optimized, a quartz crystal microbalance (QCM) was then used to study the multilayer deposition. A linear correlation between the deposited mass of $C_{12}RhMOP$ and the number of cycles is found (see Figure S8 in the Supporting Information), with an almost constant deposition of 0.31 $\mu g\cdot cm^{-2}$ for each MOP monolayer. This corresponds to 5.8 nm^2/molecule thus very similar to the area observed at the air-water interface. This accounts for the film quality, as defects in one deposition would cause poorer deposition of the subsequent monolayers.

The fabrication of MOP multilayer films with a controlled thickness offers several possibilities for the implementation of MOPs in membrane technology for gas separation. However, to our knowledge, MOPs have been only used in this field as fillers for mixed matrix membranes with micrometric thicknesses. [18-21] As a proof of concept, in order to demonstrate how the LS deposition can be used for the fabrication of MOP membranes with thicknesses in the nanometre range and supported on a porous substrate, we studied the multilayer deposition of $C_{12}RhMOP$ monolayers onto PTMSP supports. PTMSP is an ultrapermeable polymer showing very high gas permeability and low CO_2/N_2 selectivity. Moreover, it can be easily processed into very flat membranes by drop-casting (Figure 2a) and, therefore, it

is a suitable support for the deposition of LB/LS films of different substances.[8, 9]

To this end, different multilayer films were fabricated by depositing 3, 5, 10 and 20 C_{12}RhMOP monolayers onto PTMSP supports using the optimised conditions (LS deposition; surface pressure = 25 mN·m^{-1}). The resulting multilayer C_{12}RhMOP films were then characterized by AFM and X-ray photoelectron spectroscopy (XPS) (see Figure 2b, Figures S9, S11 and S12 and Table S1 in the Supporting Information). Although some small pinholes and C_{12}RhMOP agglomerations are also present, an overall good coverage of the PTMSP support is observed, even after the deposition of only three C_{12}RhMOP monolayers. The thickness of a single monolayer is estimated to be *ca.* 2.5 nm measuring the height in different film defects and borders (see Figure S7 in the Supporting Information). The size and number of film defects diminishes gradually with the number of C_{12}RhMOP monolayers transferred. An almost defect-free MOP multilayer is obtained after the deposition of *ca.* 20 LS C_{12}RhMOP monolayers.
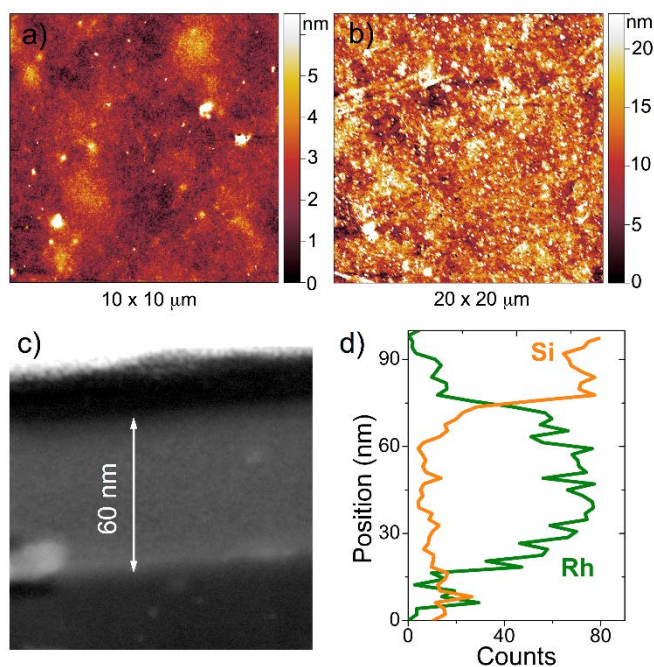

Figure 2 (a,b) AFM images of a bare PTMSP substrate (a) and a PTMSP substrate covered with 20 C_{12}RhMOP monolayers (b). (c) STEM-HAADF image from a lamella extracted from a PTMSP substrate covered with 30 C_{12}RhMOP monolayers. (d) Typical EDS signal of the Rh Lα and Si Kα peaks along the lamella profile.

To obtain a more detailed characterization of C_{12}RhMOP multilayer films deposited onto PTMSP, a lamella of a sample obtained after depositing 30 C_{12}RhMOP monolayers was extracted for analysis by scanning transmission electron microscopy (STEM). The sequence of images of the lamella thinning can be found in the Supporting Information (Figure S10). Figure 2c shows a STEM-HAADF image of the lamella in which it is possible to distinguish the MOP multilayer with a different contrast to that of the PTMSP support at the bottom and the C/Pt coatings on top. According to the images obtained, the thickness of the MOP film is close to 60-65 nm. These values are in good agreement with the thickness derived from AFM measurements (each monolayer is *ca.* 2.5 nm thick). Moreover, the composition

of the lamella was analysed by energy-dispersive X-ray spectroscopy (EDS). Figure 2d shows the Rh Lα (2.697 eV) and Si Kα (1.740 eV) peaks counts along the lamella profile, confirming the presence of Rh in the MOP multilayer film and Si in the PTMSP support. Moreover, the deduced thickness of the MOP layer derived from the EDS profiles is also consistent with the STEM-HAADF image, at *ca.* 60 nm.

The separation performance of C_{12}RhMOP supported membranes, consisting of 20 to 30 MOP monolayers deposited onto PTMSP supports was tested in CO_2/N_2 separation for post-combustion carbon capture (temperature 35°C, feed pressures 1 to 3 bar, CO_2/N_2 mixture composition 10/90 in volume). CO_2 permeance and CO_2/N_2 selectivity values for the different membranes analysed are shown in Figure 3. Pure PTMSP membranes present a high CO_2 permeance (415 GPU at 1 bar) but low CO_2/N_2 selectivity (4.2) in agreement with previous works.[9, 22]
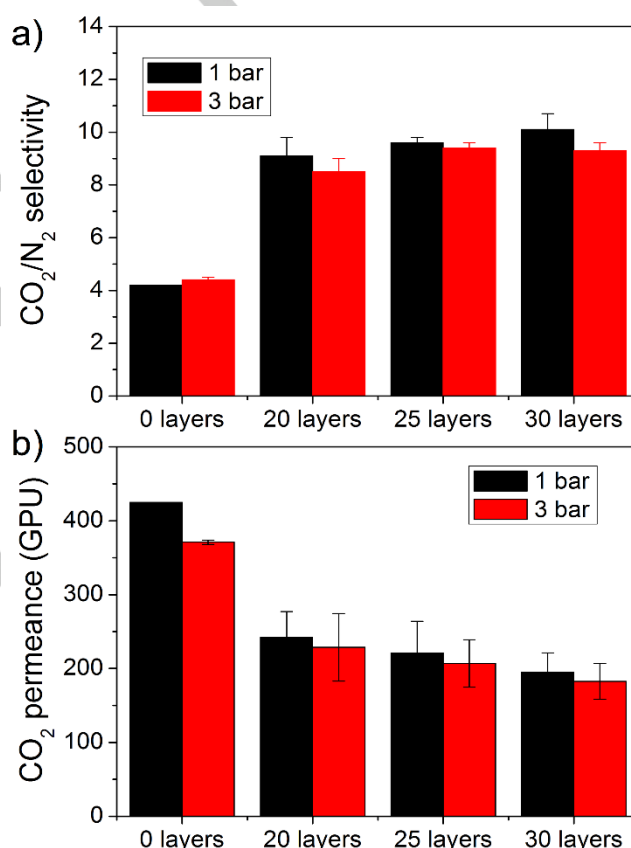
Figure 3. (a,b) CO_2/N_2 selectivity (a) and CO_2 permeance (b) of bare PTMSP (0 layers) and MOP supported membranes formed, respectively, by 20, 25 and 30 C_{12}RhMOP monolayers deposited onto PTMSP. Error bars were determined from at least 2 independent measurements.

The deposition of 20 to 30 C_{12}RhMOP monolayers increases the CO_2/N_2 selectivity at 1 bar up to values of 9.1 and 10.1 (Figure 3a), respectively, while maintaining the CO_2 permeance above 195 GPU (Figure 3b). When the feed pressure increases from 1 to 3 bar, CO_2 permeance values diminish by *ca.* 6 % for MOP supported films. However, this reduction is *ca.* 13 % for pure PTMSP supports. This difference is indicative of the formation of dense C_{12}RhMOP multilayers, as shown in STEM images.

COMMUNICATION

Comparing these data to previous studies,[9] where different polymers of intrinsic microporosity (PIMs) were deposited onto PTMSP substrates, it can be highlighted that the CO_2 permeance values obtained with 30 C_{12}RhMOP monolayers deposited onto PTMSP (195 GPU at 1 bar) are significantly higher than those obtained when stacking the same number of PIM monolayers (134 GPU for PIM-TMN-Trip films and 118 GPU for PIM-EA-TB(H_2)). However, CO_2/N_2 selectivity values are slightly lower for MOP supported films (10.1) than for PIM-TMN-Trip (12.1)[9b] and PIM-EA-TB(H_2) (13.8)[9a] supported films. This tendency is somehow expected as the higher is the permeability for a membrane, the lower is generally the selectivity.

In conclusion, we have demonstrated that the LB method can be employed to induce the self-assembly of C_{12}RhMOP into dense and ultrathin porous films, and that these films can be used as selective materials in multilayer membranes for efficient CO_2 separation. These results pave the way for the implementation of MOPs in separation technologies as the LB technique enables to fabricate large area membranes using minute amounts of active material. We believe that the versatility and ease functionalization of MOPs will provide a wide catalogue of MOP-based membranes with potential in gas separation and other applications.

Experimental Section

Thin film formation at the air-water interface

Film formation at the air-water interface (Langmuir films) was first optimized using a commercial Langmuir Teflon trough (NIMA, Model 702) with a symmetrical double-barrier configuration and dimensions of 720 × 100 mm. This device was used to register surface pressure vs. area (π-A) isotherms and Brewster angle microscopy (BAM) images. These images were obtained using a KSV NIMA Micro BAM, equipped with a red laser light source (50 mW, 659 nm) with a fixed incidence angle of 53.1º. Another apparatus (KSV-NIMA, model KN 2003) with dimensions of 580 mm × 145 mm, also equipped with a symmetrical double-barrier system, was used for the fabrication of LB and LS films onto different substrates: quartz, mica, QCM discs and PTMSP dense membranes. Both troughs were kept inside closed cabinets in a dedicated laboratory with special care to limit the presence of dust and at constant temperature (20 ± 1 ºC). Films were compressed at constant speed (8 cm²·min⁻¹). Ultra-pure Milli-Q water (ρ = 18.2 MΩ·cm) was used as subphase in all the experiments. Surface pressure was continuously registered in both devices using Wilhelmy balances with a filter paper plate.

Thin film deposition onto substrates

LB films were transferred onto solid substrates by vertical dipping at a constant speed of 1 mm·min⁻¹. For LS film fabrication, substrates were held horizontally and parallel to the water surface using a vacuum pump based horizontal dipping clamp. When the desired surface pressure was reached, the substrate was approached to the surface at a vertical speed of 1 mm·min⁻¹. Once the substrate touched the water surface, it was withdrawn at a vertical speed of 10 mm·min⁻¹. After each transfer, LS films were dried with N_2 at ambient temperature, and the procedure was repeated as many times as necessary to obtain films with the desired number of MOP monolayers.

[1]   B. Dutcher, M. Fan, A. G. Russell, *ACS Appl. Mater. Interfaces* **2015**, 7, 2137-2148.
[2]   N. Du, H. B. Park, M. M. Dal-Cin, M. D. Guiver, *Energy Environ. Sci.* **2012**, 5, 7306-7322.
[3]   V. Vrbová, K. Ciahotný, Energy Fuels **2017**, 31, 9393-9401.
[4]   M. Wang, J. Zhao, X. Wang, A. Liu, K. K. Gleason, *J. Mater. Chem. A* **2017**, 5, 8860-8886.
[5]   R. Selyanchyn, S. Fujikawa, *Sci. Technol. Adv. Mater.* **2017**, 18, 816-827.
[6]   K. Xie, Q. Fu, G. G. Qiao, P. A. Webley, *J. Membr. Sci.*, **2019**, 572, 38-60.
[7]   a) S. Motoyama, R. Makiura, O. Sakata, H. Kitagawa, *J. Am. Chem. Soc.* **2011**, 133, 5640-5643; b) M. Tsotsalas, A. Umemura, F. Kim, Y. Sakata, J. Reboul, S. Kitagawa, S. Furukawa, *J. Mater. Chem.* **2012**, 22, 10159-10165; c) R. Dong, M. Pfeffermann, H. Liang, Z. Zheng, X. Zhu, J. Zhang, X. Feng, *Angew. Chem. Int. Ed.* **2015**, 54, 12058-12063; d) S. Sakaida, K. Otsubo, O. Sakata, C. Song, A. Fujiwara, M. Takata, H. Kitagawa, *Nat. Chem.* **2016**, 8, 377-383.; e) J. Benito, S. Sorribas, I. Lucas, J. Coronas, I. Gascon, *ACS Appl. Mat. Interfaces* **2016**, 8, 16486–16492; f) V. Rubio-Giménez, M. Galbiati, J. Castells-Gil, N. Almora-Barrios, J. Navarro-Sánchez, G. Escorcia-Ariza, M. Mattera, T. Arnold, J. Rawle, S. Tatay, E. Coronado, C. Martí-Gastaldo, *Adv. Mater.* **2018**, 30, 1704291; g) V. Müller, A. Hinaut, M. Moradi, M. Baljozovic, T. A. Jung, P. Shahgaldian, H. Möhwald, G. Hofer, M. Kröger, B. T. King, E. Meyer, T. Glatzel, A. D. Schlüter, *Angew. Chem. Int. Ed.* **2018**, 57, 10584-10588.
[8]   M. Wang, V. Janout, S. L. Regen, *Acc. Chem. Res.* **2013**, 46, 2743-2754.
[9]   a) J. Benito, J. Sánchez-Laínez, B. Zornoza, S. Martín, M. Carta, R. Malpass-Evans, C. Téllez, N. B. McKeown, J. Coronas, I. Gascón, *ChemSusChem* **2017**, 10, 4014-4017; b) J. Benito, J. Vidal, J. Sánchez-Laínez, B. Zornoza, C. Téllez, S. Martín, K. J. Msayib, B. Comesaña-Gándara, N. B. McKeown, J. Coronas, I. Gascón, *J. Colloid Interface Sci.* **2019**, 536, 474-482.
[10]   J.-R. Li, H.-C. Zhou, *Nat. Chem.* **2010**, 2, 893.
[11]   C. A. Rowland, G. R. Lorzing, E. J. Gosselin, B. A. Trump, G. P. A. Yap, C. M. Brown, E. D. Bloch, *J. Am. Chem. Soc.* **2018**, 140, 11153-11157.
[12]   W.-H. Xing, H.-Y. Li, X.-Y. Dong, S.-Q. Zang, J. Mater. Chem. A **2018**, 6, 7724-7730.
[13]   M. Eddaoudi, J. Kim, J. B. Wachter, H. K. Chae, M. O'Keeffe, O. M. Yaghi, J. *Am. Chem. Soc.* **2001**, 123, 4368-4369.
[14]   S. Furukawa, N. Horike, M. Kondo, Y. Hijikata, A. Carné-Sánchez, P. Larpent, N. Louvain, S. Diring, H. Sato, R. Matsuda, R. Kawano, S. Kitagawa, *Inorg. Chem.* **2016**, 55, 10843-10846.
[15]   R. Kawano, N. Horike, Y. Hijikata, M. Kondo, A. Carné-Sánchez, P. Larpent, N. Louvain, T. Osaki, K. Kamiya, S. Kitagawa, S. Takeuchi, S. Furukawa, *Chem* **2017**, 2, 393-403.
[16]   A. Carné-Sánchez, G. A. Craig, P. Larpent, T. Hirose, M. Higuchi, S. Kitagawa, K. Matsuda, K. Urayama, S. Furukawa, *Nat. Commun.* **2018**, 9, 2506.
[17]   H. Furukawa, J. Kim, K. E. Plass, O. M. Yaghi, *J. Am. Chem. Soc.* **2006**, 128, 8398-8399.
[18]   E. V. Perez, K. J. Balkus, J. P. Ferraris, I. H. Musselman, *J. Membr. Sci.*, **2014**, 463, 82-93.
[19]   M. Kitchin, J. Teo, K. Konstas, C. H. Lau, C. J. Sumby, A. W. Thornton, C. J. Doonan, M. R. Hill, *J. Mater. Chem. A* **2015**, 3, 15241-15247.
[20]   C. R. P. Fulong, J. Liu, V. J. Pastore, H. Lin, T. R. Cook, *Dalton Trans.* **2018**, 47, 7905-7915.

[21]   X. Liu, X. Wang, A. V. Bavykina, L. Chu, M. Shan, A. Sabetghadam, H. Miro, F. Kapteijn, J. Gascon, *ACS Appl. Mater. Interfaces*, **2018**, 10, 21381-21389.
[22]   S. D. Bazhenov, I. L. Borisov, D. S. Bakhtin, A. N. Rybakova, V. S. Khotimskiy, S. P. Molchanov, V. V. Volkov, *Green Energy Environ.* **2016**, 1, 235-245.